Imaging coherent electron flow

2003 J. Phys.: Condens. Matter 15 R1835

(http://iopscience.iop.org/0953-8984/15/50/R02)

INSTITUTE OF PHYSICS PUBLISHING JOURNAL OF PHYSICS: CONDENSED MATTER

J. Phys.: Condens. Matter **15** (2003) R1835–R1863 PII: S0953-8984(03)39878-9

TOPICAL REVIEW

Imaging coherent electron flow

B J LeRoy[1]

Department of Physics, Harvard University, Cambridge, MA 02138, USA

E-mail: leroy@mb.tn.tudelft.nl

Received 8 July 2003, in final form 11 September 2003
Published 3 December 2003
Online at stacks.iop.org/JPhysCM/15/R1835

Abstract

In this review, results of imaging coherent electron flow through a two-dimensional electron gas (2DEG) are presented. The images show the modal pattern of electron wavefunctions passing through a quantum point contact. At longer distances, unexpected branching of the electron flow is observed due to the small bumps and dips in the potential caused by the donor atoms. Images of the electron flow being bent by an electrostatic prism are also presented. All of the images are decorated by interference fringes spaced by half the Fermi wavelength, which are used to spatially profile the electron density. A technique for imaging the inelastic scattering length in the 2DEG is also demonstrated.

(Some figures in this article are in colour only in the electronic version)

Contents

[1] Present address: Department of Nanoscience, Delft University of Technology, Lorentzweg 1, 2628 CJ Delft, The Netherlands.

0953-8984/03/501835+29$30.00

1. Introduction

There has been a large amount of research on the behaviour of electrons in two-dimensional electron gases (2DEG). One main focus of this research has been on the 2DEG formed at the interface of GaAs and AlGaAs, which can have a very high mobility and a wide range of densities. The research into 2DEGs has led to many important discoveries, including the integer and fractional quantum Hall effect and conductance quantization [1, 2]. Most of the work studying these systems has been done through low-temperature transport measurements, which provide information about the average behaviour of the device. However, these measurements do not provide local information about the behaviour of the electrons. Scanning probe microscopy provides information about these devices on a much smaller length scale and leads to new insights into their behaviour.

Scanning probe microscopy has been used to study a wide variety of systems at low temperatures. Some of these include imaging wavefunctions on metal surfaces [3, 4], superconductors [5, 6], semiconductors [7, 8] and carbon nanotubes [9–11] using scanning tunnelling microscopy. All of these experiments reveal information about electron wavefunctions that are on the surface of the material, but obtaining information on electrons inside semiconductor materials is more difficult. To study the electrons in semiconductor 2DEGs, new techniques are needed that can probe the electron behaviour many nanometres below the surface.

The importance of being able to understand electron phenomena on a much shorter length scale than with transport measurements has led to the development of several techniques for studying semiconductors. Some of the techniques that have been used include using the tip as a moveable scatterer [12–23], measuring the local potential [24–29] and imaging local capacitance and compressibility [30–35]. These different techniques for probing the electron behaviour have been used to study a wide range of phenomena from the quantum Hall effect to ballistic electron transport in a 2DEG.

One of the difficulties in imaging electrons buried in semiconductor heterostructures is that the separation between the tip and the electrons, which is generally more than 50 nm, can limit the spatial resolution. However, as shown in this review, using the tip as a moveable scatterer does not have this limitation and much higher resolutions can be obtained. This is especially important as the size of electronics devices continues to shrink. One of the basic devices that can be made in a 2DEG is a quantum point contact (QPC), which is a narrow one-dimensional constriction. The width of the one-dimensional channel is set by the electron wavelength, which is typically less than 50 nm. High spatial resolution is critical in order to image the electron behaviour from these devices.

The ability to probe the electron flow at low temperatures, short distances and high resolution allows the study of the quantum-mechanical nature of the electron. The electron flow through the 2DEG remains coherent as long as there is a well-defined phase relationship between the start and end of the trajectory. The high resolution of the imaging technique allows interference fringes spaced by half the electron wavelength to be observed. The persistence of the interference fringes demonstrates that the electrons are maintaining their phase relationship throughout the image and therefore the imaging technique is measuring coherent electron flow. The ability to image coherent electron flow is important in understanding new devices that rely on the coherence of the electron.

The imaging technique presented in this review uses a combination of microscopy with transport measurements. This combination provides new insights into the behaviour of electrons on a much shorter length scale than is possible with only transport measurements. It has revealed the formation of narrow branches of electron flow emanating from a QPC in a 2DEG [17]. It has also shown that the phase information of the electrons can be transmitted over distances of several microns, as evidenced by the persistence of the interference fringes. The combination has also been used to measure the electron density on a much shorter length scale than is possible with just transport measurements [36]. As new techniques become possible to image the electron flow on shorter length scales inside quantum dots and other smaller structures, more new behaviour may be discovered.

In the remainder of this review we concentrate on our work to image electron flow in a 2DEG using the tip of a SPM as a local probe of the flow. Section 2 describes the procedure that is used to image electron flow, including the sample fabrication and imaging technique. It is shown that the critical requirement in order to image electron flow with the SPM is that the tip creates a small depleted region in the 2DEG that can backscatter electron waves.

In sections 3–5, the ability of the imaging method to probe the electron flow from a QPC is discussed. Section 3 shows images of electron flow near a QPC, which demonstrate the ability of the technique to image the modal pattern of the wavefunctions and the presence of interference fringes spaced by half the Fermi wavelength. Section 4 presents the results from imaging the electron flow over a large area of the 2DEG. These large area images of the electron flow led to the discovery of narrow branches of electron flow and the persistence of interference fringes. Theoretical results for the persistence of the interference fringes and the formation of branches will be reviewed. Section 5 reviews experiments on bending the electron flow using an electrostatic gate as a prism for electron waves.

The last two sections of the review discuss other techniques that have been developed that use the SPM to investigate properties of the 2DEG. Section 6 describes a technique that is used to image the local electron density in the 2DEG based on the spacing of the interference fringes. The interference fringes are spaced by half the Fermi wavelength, which is inversely related to the electron density. Being able to spatially profile the local electron density is important for the design and characterization of new semiconductor devices.

Section 7 discusses a technique for imaging how far electrons can travel in the 2DEG without losing energy. This technique is used to measure the inelastic scattering length as a function of excess electron energy. Being able to characterize the inelastic scattering length is difficult with standard transport measurements because of the lack of spatial information. However, it is necessary to understand the energy loss mechanisms in 2DEGs in order to design new electronic devices that rely on the coherence of the electron.

2. Imaging technique

In this section, the method that is used to image the electron flow through the 2DEG is discussed. It is shown that the critical requirement in order to obtain an image is that the SPM tip depletes the electron gas and backscatters electrons. The backscattering from the SPM tip also leads to the high spatial resolution of the images. The necessary steps to fabricate the samples used in the experiments are also discussed. These steps include making ohmic contacts and depositing electrostatic gates on the surface.

2.1. Sample fabrication

The samples used for imaging electron flow are 2DEG formed at the interface of GaAs and AlGaAs. The samples are grown by molecular beam epitaxy on a conducting n-type substrate.

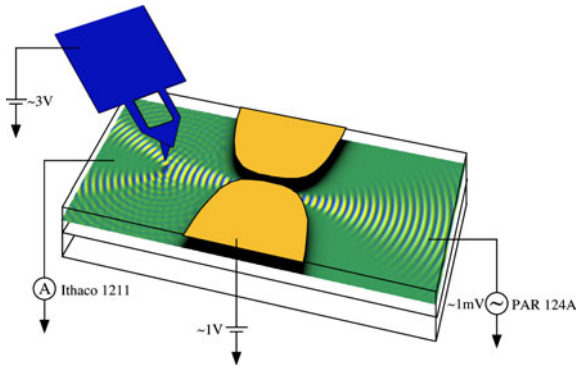

Figure 1. Schematic diagram showing the measurement set-up used to image coherent electron flow. A negative voltage is put on the tip to create a region depleted of electrons directly below. The conductance is measured between two ohmic contacts as a function of tip position using lock-in detection methods.

This allows the density of the 2DEG to be changed by applying a voltage to the substrate, which acts as a back gate. The layers, in growth order, are a smoothing superlattice, 1 μm GaAs, 22 nm AlGaAs, a δ layer of Si dopants, 20 nm AlGaAs and a 5 nm GaAs cap. This forms a 2DEG at the interface of the GaAs and AlGaAs layers 57 nm below the surface. The density of the 2DEG is 4.2×10^{11} cm^{-2}, giving a Fermi wavelength of 39 nm. The mobility of the 2DEG is 1.0×10^{6} cm^{2} V^{-1} s^{-1}, giving a mean free path of 11 μm. The long mean free path means that all of the measurements discussed in this review are in the ballistic regime.

To create the devices ohmic contacts and electrostatic gates are defined by electron-beam lithography. Ohmic contacts are fabricated to measure the conductance through the 2DEG. The ohmic contacts consist of a mixture of Ni, Au and Ge, which is diffused into the sample to make contact with the 2DEG. A mesa is defined to separate the active region of the device from the connection to the back gate, allowing separate control of the conductance through the device and the voltage on the back gate. Cr and Au electrostatic gates are then deposited to make the devices.

2.2. Imaging technique

The method of imaging electron flow uses the SPM tip as a moveable gate that scatters electron waves. The tip backscatters some of the electron waves, reducing the conductance. When the tip is over an area of high electron flow, there is a large amount of backscattering and hence a large decrease in conductance. However, when the tip is over an area of little flow, there is a correspondingly small change in conductance. By measuring the change in conductance as a function of tip position, an image of electron flow is obtained.

Figure 1 is a schematic diagram showing the set-up used to image electron flow. The conductance of the device is measured between two ohmic contacts far away, which are not shown. The conductance is measured using lock-in detection methods with an ac frequency of about 10 kHz across the QPC. The QPC gate is energized negatively with respect to the 2DEG, creating a narrow channel through which the electrons must flow. A negative voltage is put on the tip, which depletes the electrons below. Figure 2 shows an example of an image of electron flow obtained with this technique. The image shows the electron flow coming from a QPC off the right side of the scan. The blue areas are areas of high electron flow while the black are areas of no electron flow. The image is decorated by interference fringes spaced by

half the Fermi wavelength, which are present throughout the scan area. All of the experimental images presented in this review are taken at a temperature of 1.7 K.

The most important requirement for obtaining an image with this method is that the voltage on the tip is sufficient to deplete the electron gas below [37]. Figure 3 shows the effect of making the voltage on the SPM tip more negative. Going from figures 3(a) to (f), the voltage on the tip decreases from -1.5 to -4.0 V in steps of 0.5 V. There is no change in conductance until the tip first depletes the electron gas and then the signal quickly increases. There is no image of electron flow in figures 3(a) and (b) since the voltage on the tip is too small and there is no backscattering from the tip. Once the tip is making a depletion region the image of electron flow is obtained. In figures 3(d)–(f), there is little change in the image as a function of tip voltage. This is because the tip's depletion region is just growing but not changing whether it backscatters. This also shows that the size of the depletion region does not affect the image of electron flow, providing evidence that we are imaging the flow that was present without the tip. This shows that the size of the depletion region does not affect the spatial resolution and therefore the separation between the tip and the 2DEG does not limit the resolution. The requirement of having an area depleted of electrons has been confirmed by quantum mechanical simulations [38].

Figure 4 illustrates the importance of the depleted region in order to acquire images of electron flow. If the tip just creates a bump in the potential felt by the electrons, it will not backscatter electrons as shown in figure 4(a). This is because the electrons still have enough energy to go over the bump and therefore will not be reflected back to the QPC but will be at most bent. However, if the voltage is increased so that the bump reaches the height of the Fermi energy, as in figure 4(b), there is a region of depleted electrons. This area is classically forbidden for the electrons and electron waves impinging on it will be backscattered. This will scatter some of the electrons back through the QPC, which reduces its conductance. Since the measurement is only sensitive to changes in conductance this produces an image of electron flow, while the first case does not give any signal.

The depletion region is also important for the high resolution of our technique. Since the 2DEG is located 57 nm below the surface and the tip is at least a few nanometres above the surface, the distance from the tip to the 2DEG is at least 60 nm. This distance sets the half-width of the perturbation caused by the tip in the 2DEG. However, we are easily able to resolve features that are much smaller than this size, as evidenced by the narrow branches of electron flow and the interference fringes. Figure 4(c) illustrates how this high spatial resolution is achieved from the large depletion region below the tip. The tip acts as a hard wall scatterer, meaning that the angle of incidence of a wave is the same as the angle of reflection. Therefore only an electron wave that hits normal to the tip will be directly backscattered. All the other angles will be scattered but eventually make it to the ohmic. The red path that is directly backscattered can return back through the QPC and reduce its conductance. The small spot on the tip that backscatters electrons to the QPC determines the resolution as opposed to the entire width of the perturbation. This gives the high resolution image from the relatively blunt probe. By oscillating the voltage on the tip, the location of the backscattering from the tip changes, giving an image that is the spatial derivative of the electron flow [39].

3. Electron flow near a QPC

One of the basic devices that can be made in a semiconductor 2DEG is a QPC. Understanding the pattern of electron flow from QPCs is important because they are fundamental elements in many more complicated semiconductor devices like quantum dots. Figure 5(a) is a scanning electron microscope image of a QPC device. The QPC is formed by two lithographically

patterned electrostatic gates on the surface of the semiconductor heterostructure, which confine the electrons to a one-dimensional channel. The confinement of the electrons to one dimension leads to a quantized conductance through the QPC [40, 41]. The number of quantum mechanical modes accessible inside the QPC determines its conductance and also the pattern of electron flow through it. Figure 5(b) plots the conductance through the QPC as a function of its width controlled by the gate voltage. The quantized conductance plateaus are clearly visible at integer multiples of $2e^2/h$.

The conductance of the QPC can be calculated using Landauer–Buttiker formalism if the transmission probabilities of each mode are known [42–44]. The conductance, G, is given by the following equation:

$$G = \frac{2e^2}{h} \sum_i T_i$$

where the summation is over all of the modes of the QPC and the T_i are the transmission probabilities of the individual modes through the QPC. At zero temperature, if there is no scattering in the QPC, the transmission probability is either 0 or 1 for each of the modes. This shows that the conductance is quantized in units of $2e^2/h$, depending on the number of modes accessible in the QPC.

Images of electron flow from the QPC show modal patterns characteristic of the individual modes of the wavefunction in the QPC [13]. There is one lobe for the first mode, two for the second and three for the third mode. This is in agreement with quantum mechanical simulations of the pattern of electron flow from a QPC. The images of electron flow also show interference fringes spaced by half the electron wavelength, demonstrating that the electron flow is coherent. Inside the QPC channel experimental and theoretical images of electron flow also show the modal features of the wavefunctions [16, 45].

Figure 6 shows the electron flow from the first three plateaus of a QPC. Figure 6(a) shows the electron flow from the first plateau of the QPC, which has one main lobe. The conductance through the QPC is $2e^2/h$ and one mode is accessible inside the QPC. Figure 6(b) shows the flow from the second plateau, which has contributions from both the first and second modes of the QPC. Figure 6(c) is an image of the electron flow from the third plateau of the QPC, with contributions from the first three modes of the QPC. As the width of the QPC is increased, new lobes of current are added at each plateau of the QPC. All three images are decorated by interference fringes spaced by half the Fermi wavelength, showing that the flow is coherent. The fringes are spaced by 20 nm showing the high resolution of the imaging technique.

A large ac voltage applied across the QPC blurs out the interference fringes due to the large range of electron energies contributing to the signal. Figure 7 shows the effect of applying a large ac voltage of 3.0 mV across the QPC. The top row of figure 7 shows the pattern of electron flow from the first three plateaus with a small ac voltage of 0.2 mV. These images show the coherent interference fringes. The bottom row of figure 7 shows the electron flow with a large ac voltage applied. The interference fringes are no longer visible in the image but the underlying pattern of electron flow has remained unchanged. This shows that the ac voltage destroys the interference but does not affect the pattern of electron flow.

The modal pattern of the wavefunctions from the individual modes of the QPC can be extracted from the images of electron flow. Figures 8(a)–(c) are images of the individual modes of the QPC. They were obtained from images of electron flow by the following procedure. Figure 8(a) is the image of electron flow from the first plateau of the QPC since it only contains a contribution from the first mode. Figure 8(b) is the difference between the image of electron flow on the second plateau (figure 7(e)) of the QPC and the one from the first plateau (figure 7(d)). This yields only the contribution from the second mode of the QPC because the

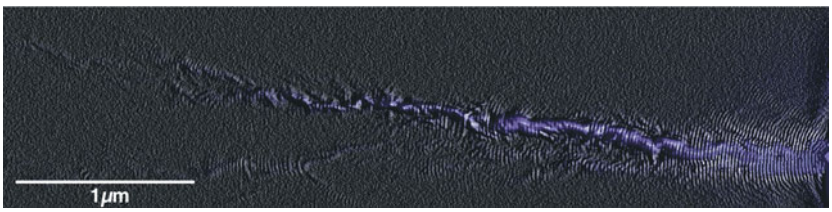

Figure 2. Example of an image of electron flow. Areas of high flow are show in blue while black indicates little or no flow. Interference fringes spaced by half the Fermi wavelength are present, indicating that the flow is coherent. The image is taken at a temperature of 1.7 K.

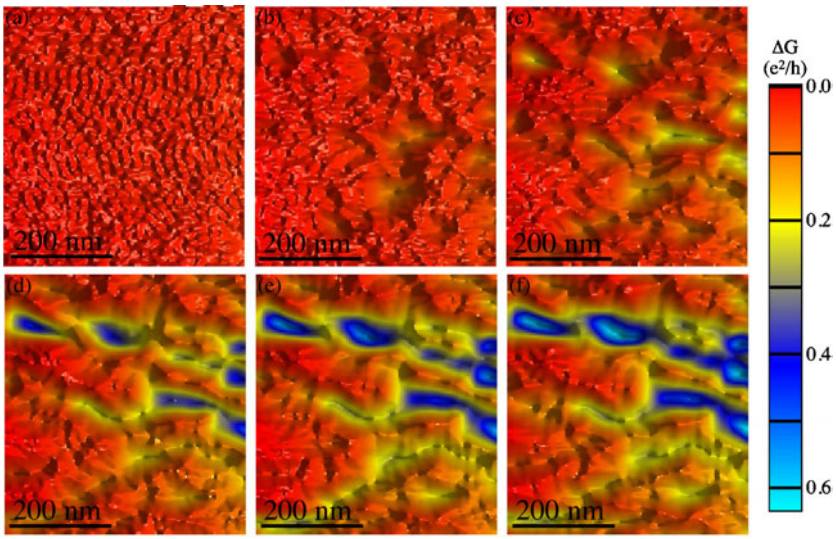

Figure 3. Images of electron flow as a function of tip voltage. The tip voltage in each image is as follows (a) −1.5 V, (b) −2.0 V, (c) −2.5 V, (d) −3.0 V, (e) −3.5 V and (f) −4.0 V. Images of electron flow are only possible when the 2DEG is depleted beneath the tip as in (d)–(f).

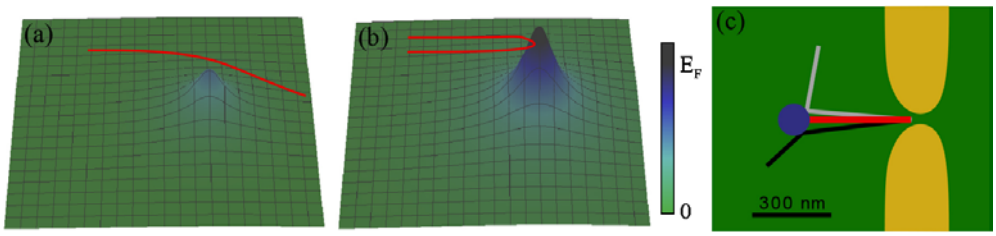

Figure 4. (a) Diagram showing the trajectory taken by an electron when the voltage on the tip is not sufficient to deplete the 2DEG. (b) The voltage on the tip depletes the 2DEG backscattering electrons, producing an image of electron flow. (c) Schematic showing how the high spatial resolution is obtained from the tip. Only the path that hits the tip directly (red) and is backscattered through the QPC reduces its conductance. All of the other paths still make it to the ohmic contact. This means that only a small area of the perturbation from the tip is used to create the images.

image from the second plateau contains contributions from the first and second modes while the image from the first plateau contains a contribution from the first mode. Figure 8(c) was obtained in a similar manner by subtracting an image of the electron flow on the second plateau

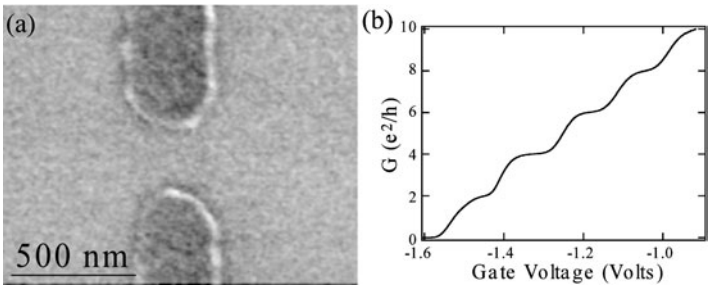

Figure 5. (a) Scanning electron microscope image of a QPC device. (b) Conductance through the QPC as a function of its gate voltage taken at a temperature of 1.7 K. Conductance plateaus at integer multiples of $2e^2/h$ are visible.

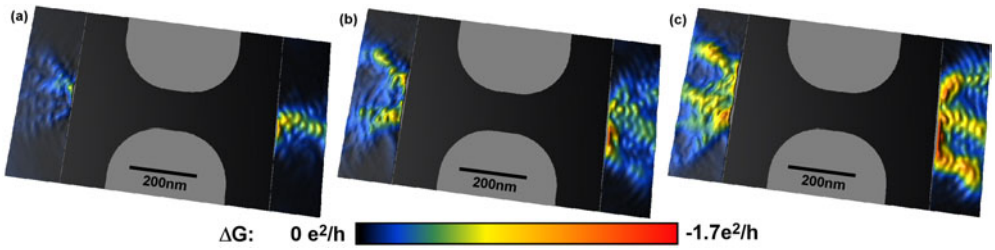

Figure 6. Images of coherent electron flow from the (a) first, (b) second and (c) third plateau of a QPC. These show the modal pattern of the electron flow changing as the width of the QPC is increased. Interference fringes spaced by half the Fermi wavelength are present in all three images. Reprinted with permission from [13]. Copyright 2000 American Association for the Advancement of Science.

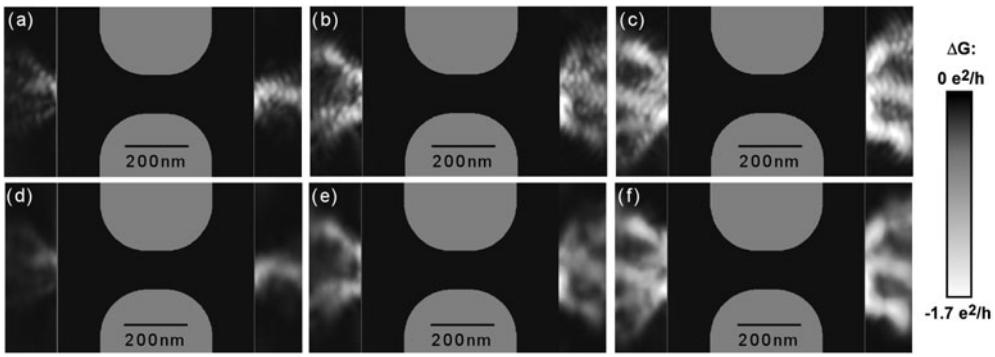

Figure 7. (a)–(c) Images of electron flow from the first three plateaus of a QPC with a small ac voltage across the QPC, 0.2 mV. (d)–(f) These show the effect of heating the electrons using a large ac voltage across the QPC, 3.0 mV. This shows that the interference fringes are blurred out by the large ac voltage but the pattern of electron flow remains unchanged. Reprinted with permission from [13]. Copyright 2000 American Association for the Advancement of Science.

from one on the third plateau. These images show that each new mode of the QPC has an additional lobe of current. There is one lobe for the first mode, two for the second, etc.

Figures 8(d)–(f) are simulations of the electron flow for the first three modes of a QPC. The outline of the gate is shown by the grey line, which indicates where the potential crosses

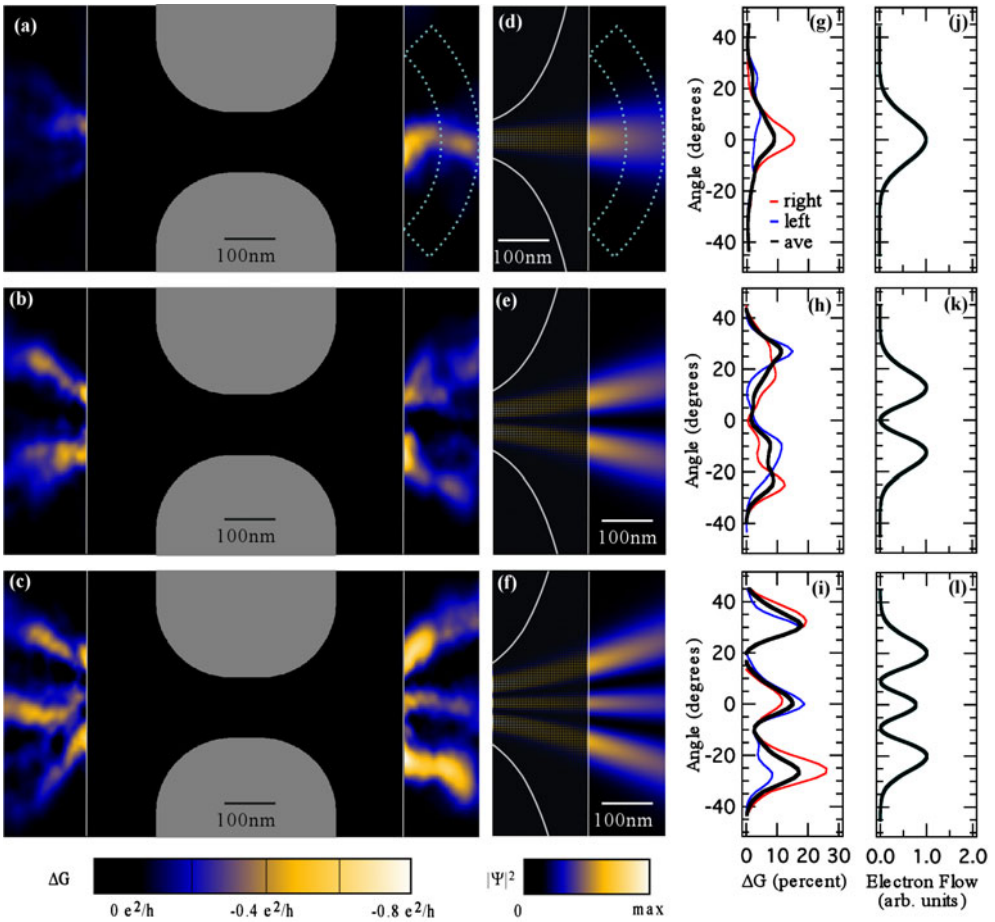

Figure 8. (a)–(c) Experimental images of the wavefunctions of electrons passing through the first three modes of a QPC. See the text for an explanation of how these are obtained from the images of electron flow. (d)–(f) Theoretical simulations of the wavefunctions for the first three modes of the QPC. (g)–(i) Angular distributions taken for the experimental images in (a)–(c). (j)–(l) Angular distributions taken from the theoretical simulations in (d)–(f). In both the experimental and theoretical images the number of lobes of current is equal to the mode number of the QPC: one lobe for the first mode, two lobes for the second mode, etc. Reprinted with permission from [13]. Copyright 2000 American Association for the Advancement of Science.

the Fermi energy. There is fairly good agreement between the simulated wavefunctions and the experimental images. There has been no fitting done to match the shape of the potential with the profile of the gates in the experiment. There is one main lobe in the wavefunction for the first mode, two for the second and three for the third. This is in agreement with the experimental results, which show that the number of lobes is equal to the mode number of the QPC.

Figures 8(g)–(l) plot the angular dependence of the wavefunctions for both the experiment and the simulations. The plots were acquired by taking an average over the region outlined by light blue in figures 8(a) and (d). Once again the plots show good agreement between experiment and theory. The number of lobes of current agrees between experiment and theory and also matches the mode number of the QPC. Furthermore, the overall width of the electron flow is very similar in both cases.

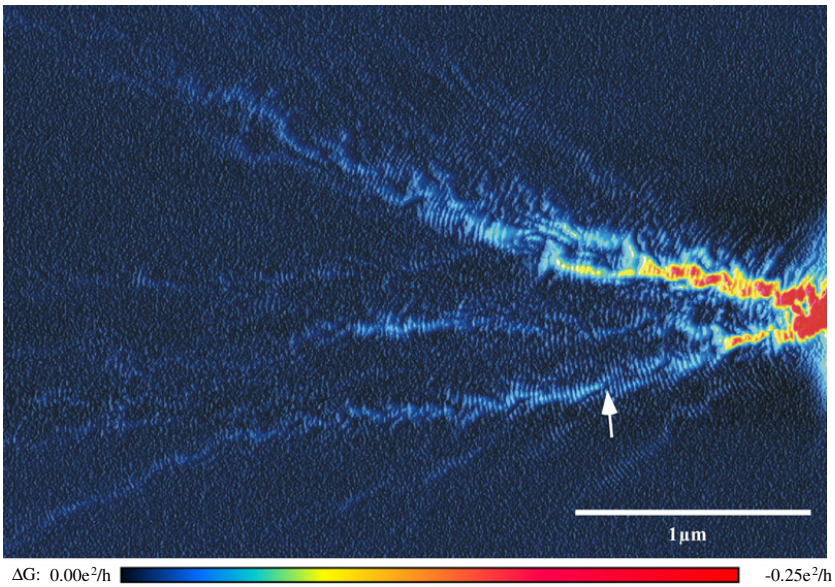

Figure 9. Image of electron flow from a large area of the 2DEG. The QPC is located about 500 nm to the right of the image. The electron flow forms narrow branches due to the cumulative effect of many small-angle scattering events. The white arrow indicates the location of a caustic formed by a small dip in the potential. The interference fringes persist throughout the image, showing that the flow is coherent. This figure was reproduced with permission from [17]. Copyright 2001 Nature Publishing Group, www.nature.com.

Images of electron flow near a QPC show the modal pattern of the wavefunction inside the channel. The number of lobes of current is equal to the mode number of the QPC. Interference fringes spaced by half the Fermi wavelength arising from constructive and destructive backscattering from the SPM tip have also been observed.

4. Electron flow through a 2DEG

Images of electron flow from a QPC acquired over a large area reveal the dynamics of the electron flow through the 2DEG. These images of electron flow are necessary to understand the behaviour of electrons as they travel through the 2DEG. The images show unexpected branching of the flow due to the small bumps and dips in the potential caused by the ionized donor atoms [17]. These narrow branches are a general result of travelling through a slowly varying potential and have been observed in many other areas, including sound propagation through the ocean [46]. There have been several theoretical studies of electron flow through a random potential using classical, semi-classical and quantum mechanical methods to understand the dynamics and statistics of the electron flow [17, 47, 48]. Interference fringes spaced by half the Fermi wavelength decorate the images and persist throughout. The persistence of the fringes is due to interference between backscattering from the tip and backscattering from impurities at the same distance from the QPC as the tip [49, 50].

Figure 9 is an image of the electron flow from the first mode of a QPC. The QPC is located about 500 nm to the right of the image. This image extends out from the QPC more than 3 μm, whereas the images in the previous section were all within 1 μm of the QPC. Narrow branches of electron flow are visible throughout this image. The intensity of the image falls off as $1/r^2$

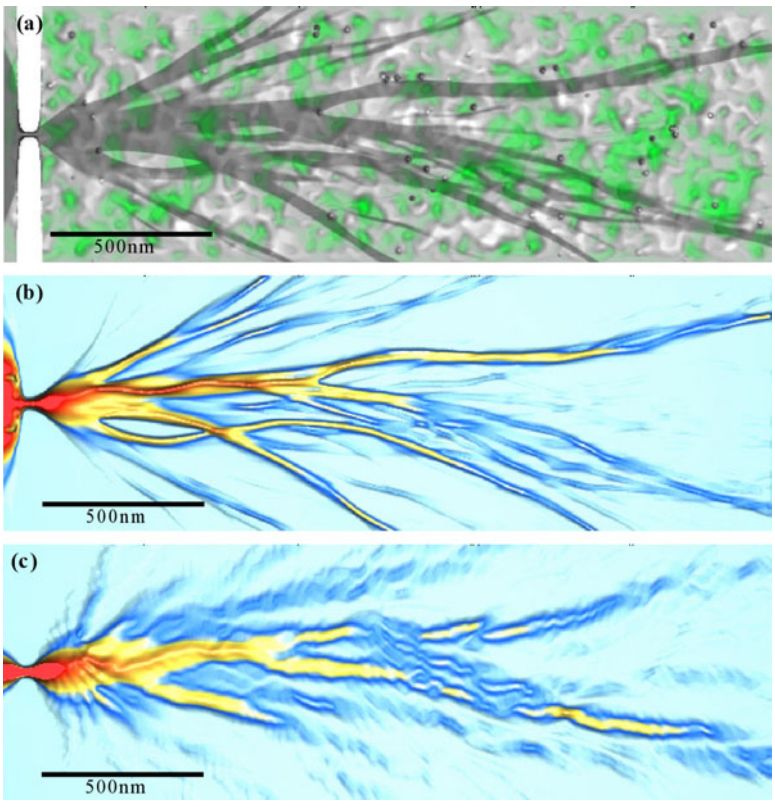

Figure 10. (a) Simulation of the potential felt by electrons passing through the 2DEG. Green areas are low spots while white ones are high. There is a variation of about 20% of the Fermi energy in the potential. (b) Quantum mechanical simulation of the electron flow through the potential in (a). The grey shadow in (a) is the quantum mechanical simulation showing that the electrons travel over both high and low areas of the potential. (c) Classical simulation of the electron flow through the potential in (a). This reproduces the formation of the narrow branches of current, showing they are a classical effect. This figure was reproduced with permission from [17]. Copyright 2001 Nature Publishing Group, www.nature.com.

due to a $1/r$ decrease in the wave going towards the tip and another $1/r$ decay on the return from the tip to the QPC [51]. However, the relative strength of the interference fringes persists throughout the image. The fringes demonstrate that the flow is coherent and can be used as a measure of the local electron density, as discussed in section 6.

The narrow branches of electron flow are formed by the cumulative effect of many small-angle scattering events. The potential landscape felt by the electrons passing through the 2DEG is not flat but rather is slowly varying due to the random ionization of Si donor atoms and impurities [52, 53]. Figure 10(a) plots a simulation of the potential in the 2DEG showing the small bumps and dips. This potential gives the same values for the standard bulk measurements, like mobility and density, as the samples used in the experiment. The variations in the potential are randomly distributed with a maximum size of about 20% of the Fermi energy. The electrons are not forced to flow through low spots in the potential but rather can go over low and high areas. Figure 10(b) is a quantum mechanical simulation of the electron flow through this potential. This shows the narrow branches of electron flow seen in the experimental images of electron flow. The grey shadow in figure 10(a) is the pattern of electron flow from the

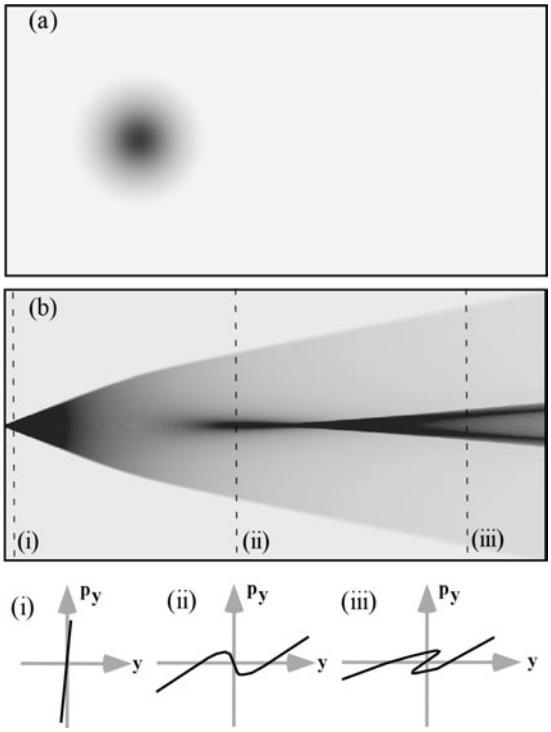

Figure 11. (a) Plot showing the location of a dip in the potential felt by electrons. (b) Plot of the classical trajectories of electrons passing over a dip in the potential, showing the formation of two caustics. (i), (ii), (iii) Plots of the y–p_y phase space at the three locations indicated. The two folds in phase space lead to the caustics seen in the plot of the electron flow.

quantum mechanical simulation showing that the flow does not just follow the low points in the potential. The flow is not being guided like water through a river valley but rather it is being slightly bent and focused by the small bumps and dips. Figure 10(c) is a classical simulation of the electron flow, which shows the same qualitative features as the quantum mechanical simulation. This leads to the conclusion that the formation of the branches of electron flow is a classical effect.

The branches of electron flow are due to caustics in the electron flow caused by the small dips in the potential. Figure 11 illustrates how a dip in the potential leads to the formation of two branches of electron flow. Figure 11(a) is a potential with just one dip and figure 11(b) shows the electron flow pattern from this single dip. In this example, electrons all start from the same position with a spread in their y momentum, as shown by the y–p_y phase space plot labelled (i). As the electrons near the dip the ones passing above are bent downwards, reducing their y momentum. The opposite is the case for the ones passing below the dip. This leads to two groups of electrons all occupying the same y position but having a spread in y momentum as shown in (ii). Once these branches of electron flow are formed they are stable and persist, as shown by them moving apart in (iii). The actual potential felt by electrons in the 2DEG includes many dips leading to the many branches of electron flow. One of the caustics is indicated by the white arrow in figure 9.

These images of electron flow show that the trajectories taken by electrons travelling through the 2DEG are complicated. The electrons are bent and focused even within distances

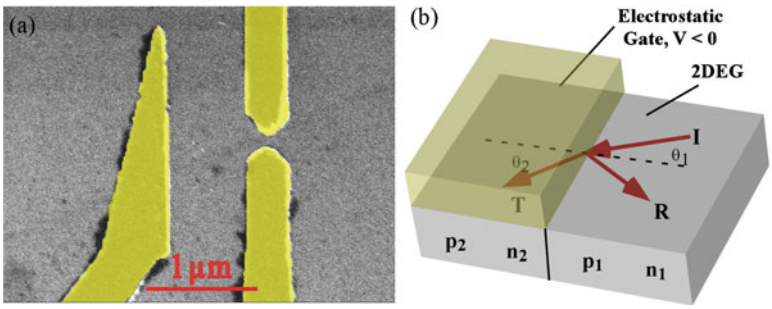

Figure 12. (a) Scanning electron microscope image of the electrostatic prism device. It consists of a QPC on the right and a triangular shaped prism gate located 1 μm to the left. (b) Schematic diagram showing what happens to an incoming electron wave when it hits the region of reduced density under the prism gate. The electron trajectory is bent away from the normal.

much shorter than the mean free path. This is caused by the small variations in the potential due to the random ionization of Si donor atoms. The electrons still remain coherent after these scattering events, as evidenced by the persistence of the interference fringes.

5. Electrostatic prism

Electron-optic devices have been studied for many years in 2DEGs [54]. These devices rely on the ballistic transport of the electron from an injector to a collector. As the mobility of 2DEGs improves and hence their mean free path increases, the size of the devices can increase. Some of the devices that have been studied are an absorber [55], a switch [56], a lens [57], a beam crosser [58] and an elliptical reflector [59]. None of these devices work as well as expected for ideal ballistic flow of electrons due to the small background potential of the donor atoms, which leads to small-angle scattering. The potential profile of the electrostatic gates can also degrade the performance of the devices. By studying these devices with an imaging technique the pattern of electron flow is obtained and the effect of the donor atoms and electrostatic gates can be understood.

In this experiment, an electrostatic prism is used to control the direction of electron flow in the 2DEG. Figure 12(a) is a scanning electron micrograph of the device used in the experiment. It consists of a QPC on the right and a wedge-shaped electrostatic gate that acts as a prism. The front edge of the prism gate is located 1 μm to the left of the QPC. The voltage on this prism gate controls the direction of electrons as they leave the area under the gate. Figure 12(b) illustrates the idea behind using an electrostatic gate to change the direction of electron flow. There are two different regions of the 2DEG: one that has a gate on it and another that does not. A voltage is put on the gate, which changes the density of the 2DEG underneath and also the momentum of the electrons. As electrons travel through the ungated 2DEG and impinge on this area of changed density, they must conserve their momentum along the interface between the two regions. This means that all of the change in momentum occurs along the axis normal to the interface and the direction of the electron is changed. The equation for the conservation of momentum gives the following simple relation between the incoming and outgoing angle of the electron:

$$p_1 \sin(\theta_1) = p_2 \sin(\theta_2)$$

where p_1 and p_2 are the incoming and outgoing momenta and θ_1 and θ_2 are the two angles.

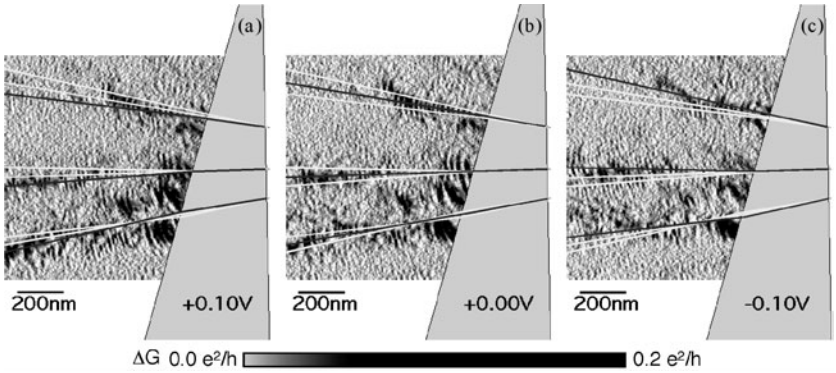

Figure 13. Three images of electron flow for different voltages on the electrostatic prism gate: (a) +0.1 V, (b) 0.0 V and (c) −0.1 V. The lines on the images represent the expected direction of electron flow for the three different gate voltages. The black line is the direction for the given image. As the voltage on the prism is made more negative the electron flow is directed more upwards. This figure was reproduced with permission from [60]. Copyright 2002 IOP Publishing Limited.

Using the fact that the square of the momentum in the 2DEG is proportional to the density, this equation can be rewritten as

$$\sqrt{n_1}\sin(\theta_1) = \sqrt{n_2}\sin(\theta_2)$$

where n_1 and n_2 are the densities in the two different regions. In this form, it is clear that this is just an electron analogue of Snell's law in optics, where the density of the 2DEG is analogous to the index of refraction. When an electron goes from an area of low density to one of higher density it will be bent towards the normal.

Images of electron flow after travelling under the prism gate have been acquired for a series of different voltages on the gate [60]. As the voltage on the gate is made more negative, the density is reduced, causing the flow to bend towards the normal. This is the opposite of light entering vacuum from glass where the light bends away from the normal. This type of device can be used as a switch to control the flow of electrons [56]. A change in the voltage on the prism changes where the electrons go. If there are two collectors then the electron flow can be shifted from one to the other, causing the current to switch. We are able to change the density under the prism from slightly above the density of the 2DEG all the way down to 0. When the density is reduced the electrons can no longer pass under the gate and all of the flow is reflected at the front edge of the prism.

Figure 13 shows three images of electron flow from the prism device for (a) +0.1 V, (b) 0.0 V and (c) −0.1 V on the prism. These images were taken on the second plateau of the QPC giving three main lobes of current. The images show the flow bending upwards as the voltage is made more negative on the gate. The lines on the images are the expected bending of the electrons for the three different prism voltages shown. The dark line on each image is the expected bending for that voltage, while the white lines are the bending for the other two voltages. This shows fairly good agreement between the measured bending of the electron flow and the expected bending.

To further emphasize the change in flow with prism voltage, figure 14 shows two images of coherent flow at different prism voltages subtracted from each other. This highlights the difference between the two images. We have subtracted the image of electron flow with −0.1 V on the prism image, figure 13(c), from one with +0.1 V, figure 13(a). The areas in red are stronger in the −0.1 V image while the blue areas are stronger in the +0.1 V image. The white

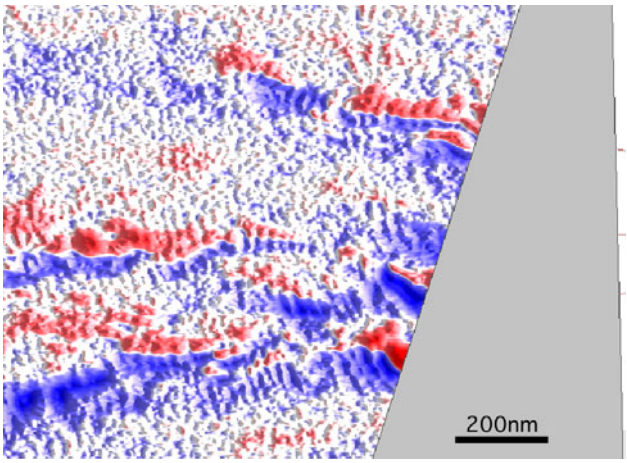

Figure 14. Image showing the effect of changing the prism gate voltage. The red areas are stronger when the gate voltage is −0.1 V and the blue areas are stronger when it is +0.1 V.

areas were the same in both images, showing that there is no change in the current. This shows that the flow bends upwards when the voltage is made more negative.

The operation of an electrostatic prism in a 2DEG has been demonstrated by imaging the coherent electron flow that passes under the prism gate. These images show how the prism can be used as a coherent switch for electrons by adjusting the voltage on its gate. It can also be used as an energy-selective scatterer for a fixed voltage on the gate because the amount of bending depends on the electron energy.

6. Imaging local electron density

This section describes the results of experiments to image local electron density. Section 6.1 describes the sample structure and basic device properties including the effect of the back gate on the electron density. Section 6.2 discusses the imaging technique and presents images of coherent electron flow for different back gate voltages. Section 6.3 details the data analysis procedures used to extract the density from an image of electron flow. The results for the local electron density are compared with the expected density using a parallel plate capacitor model and Shubnikov–de Haas measurements. The last section 6.4 describes results of mapping the electron density in the 2DEG.

The local electron density in the 2DEG is measured by imaging the coherent electron flow from a QPC [36]. The images show the pattern of electron flow and are decorated by interference fringes spaced by half the Fermi wavelength. The spacing of these fringes is a measure of the local electron density. The fringes arise from interference between backscattered paths from the tip to the QPC. As the position of the tip is changed the path length changes and the interference goes from constructive to destructive and back to constructive. If the tip is moved a distance d from one constructive interference peak to the next one, the phase accumulated along this path is 2π and must equal $2dk_{\mathrm{F}}$, where k_{F} is the magnitude of the local Fermi wavevector. In this way, the spacing of the interference fringes measures the local value of the Fermi wavevector.

The technique discussed in this section can be used to profile the electron density distribution in new 2DEG devices. Small changes in the local density can be resolved because

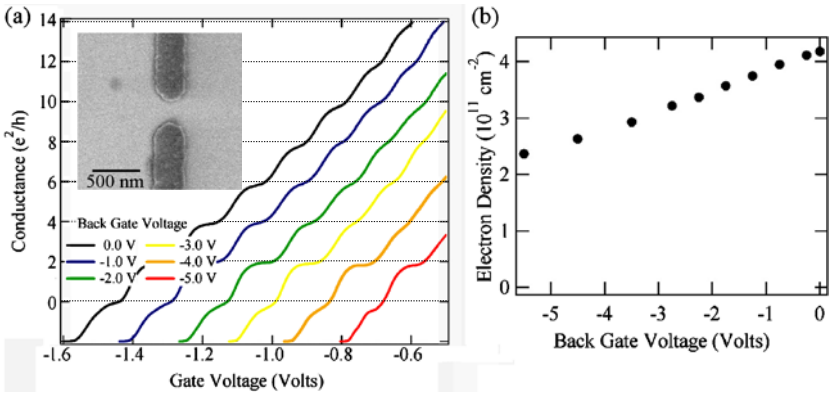

Figure 15. (a) Conductance through the QPC as a function of the voltage on its gate. This shows clear conductance plateaus at multiples of $2e^2/h$. A variety of back gate voltages are plotted showing the decreasing density of the 2DEG. The inset shows a scanning electron micrograph of a typical QPC device used in the experiments. (b) Measured density as a function of back gate voltage, showing a linear decrease in density. This measurement was done using Shubnikov–de Haas oscillations on another piece of the same wafer as used in the imaging experiments.

of the high resolution of the images. The spatial resolution of the technique can profile changes in the local electron density on a length scale of about 100 nm. This scale is set by the requirement that we take the Fourier transform over several wavelengths in order to obtain precise density information.

6.1. Sample design and characterization

In this experiment, QPC devices are fabricated in GaAs/AlGaAs heterostructures. The inset to figure 15(a) shows a scanning electron micrograph of one of the devices. A negative voltage is put on the QPC gates with respect to the 2DEG to create a variable width channel through which the electrons must flow. The n-type conducting substrate is used as a back gate for the devices. The back gate is located about 2 μm below the 2DEG, allowing the density to be modified using a fairly small voltage.

Figure 15(a) shows the measured conductance through the QPC as a function of the voltage on its gate for a series of back gate voltages. This shows conductance steps at multiples of $2e^2/h$ as found previously [40, 41]. The steps are due to each new quantum mode of the QPC becoming accessible as its width is opened. As the back gate voltage is made more negative, the gate voltage required to pinch off the QPC is less. This is caused by the density being reduced and because the width of the constriction must be larger for the electrons to get through since their wavelength is increasing. As the density is reduced, the plateaus no longer lie exactly on multiples of $2e^2/h$. This is due to increased backscattering near the QPC, which reduces its conductance. The plateaus are also not as well defined as the density decreases because the energy spacing between subbands of the QPC decreases. The reduced subband spacing, along with the temperature of the measurement, allows electrons to travel through multiple subbands, causing the plateaus to blur.

Before measuring the local electron density with the imaging technique, the effect of the back gate on the average density of the 2DEG has been characterized. To study the effect of the back gate voltage on the density, the density of the 2DEG has been measured using Shubnikov–de Haas oscillations. With a large perpendicular magnetic field applied to the

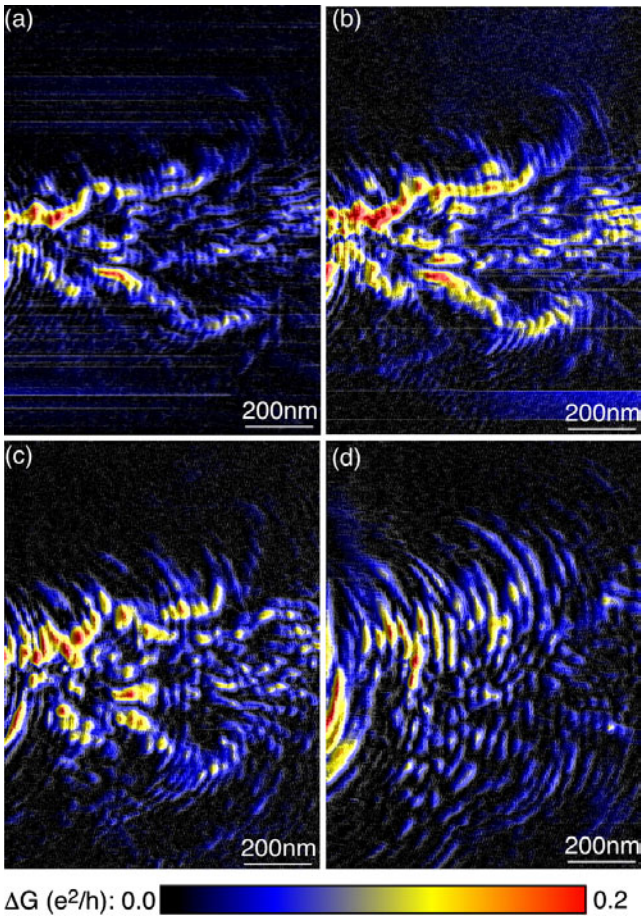

Figure 16. Four images of electron flow from the QPC for different back gate voltages: (a) −0.0 V, (b) −1.0 V, (c) −3.0 V and (d) −5.0 V. These show the spacing of the interference fringes increasing and the flow becoming more diffuse. This figure was reproduced with permission from [36]. Copyright 2002 American Institute of Physics.

sample, the constant two-dimensional density of states becomes a series of sharp peaks centred at the Landau levels. The positions of the Landau levels are given by $E_n = (n + 1/2)\,\hbar\omega_c$, where ω_c is the cyclotron frequency, $\omega_c = eB/m$. The Shubnikov–de Haas oscillations occur as each successive Landau level is emptied by increasing the magnetic field. There is a dip in the longitudinal resistance when the Fermi energy equals the energy of the Landau level, giving oscillations that are periodic in the inverse magnetic field. Their period gives the density of the 2DEG using the formula $n_s = 2e/(h\Delta(1/B))$, where e is the electron charge, h is Planck's constant and $\Delta(1/B)$ is the period of the oscillations. This measurement was repeated for a series of back gate voltages, which reduce the density. Figure 15(b) shows the effect of the back gate voltage on the average density. Each of the Shubnikov–de Haas measurements gives one of the data points in the plot of density versus back gate voltage. These data were taken from a different piece of the same wafer as used in the imaging experiment. To further investigate the reduction in density, images of the electron flow as a function of back gate voltage have been acquired.

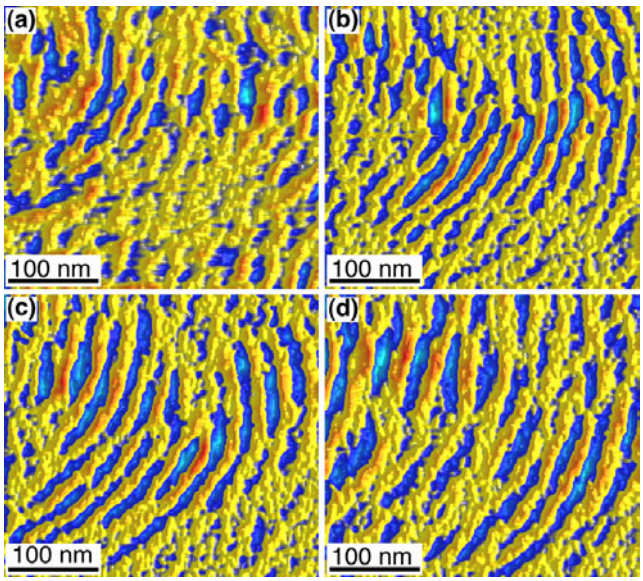

Figure 17. Images of the interference fringes for four different back gate voltages: (a) 0.0 V, (b) −1.0 V, (c) −3.0 V and (d) −5.0 V. These images are from a small section of the images in figure 16 and have been spatially high pass filtered. This figure was reproduced with permission from [36]. Copyright 2002 American Institute of Physics.

6.2. Imaging electron flow

Scanning probe microscopes can provide information about mesoscopic devices on a length scale not accessible with standard transport measurements. In this section, the local density of electrons is probed using a scanning probe microscope. This gives the density on a 100 nm length scale. Compare this with a standard Shubnikov–de Haas measurement of density that yields the average density over the entire sample but does not give any local information. The ability to image the density on these short length scales is important for the design of new mesoscopic devices. This technique can also be used to probe the density in new semiconductor heterostructures. Recently a new technique using Kelvin probe microscopy has been demonstrated, which is able to measure the electron density in the 2DEG with high spatial resolution [61].

The experimental set-up used to measure the local electron density is the same set-up that is used to acquire images of electron flow. The one important aspect to note is that the samples used in this experiment have a back gate that allows the density to be changed. This provides an experimental degree of freedom that gives a check for the measurements. By scanning the tip over the sample and measuring the conductance as a function of position, an image of electron flow is obtained. The images are decorated by interference fringes spaced by half the Fermi wavelength, whose spacing is used to measure the local electron density.

Figure 16 shows four images of electron flow from the QPC for four different back gate voltages. The back gate voltage in the four images is (a) 0 V, (b) −1 V, (c) −3 V and (d) −5 V. These images show how the electron flow changes with back gate voltage. The spacing of the interference fringes that decorate the images increases as the back gate voltage decreases. This occurs because the fringes are spaced by half the Fermi wavelength, which is being increased by the decreasing density. The second change as the back gate voltage decreases is that the strength of the branches of flow becomes less pronounced. This is due to the flow becoming

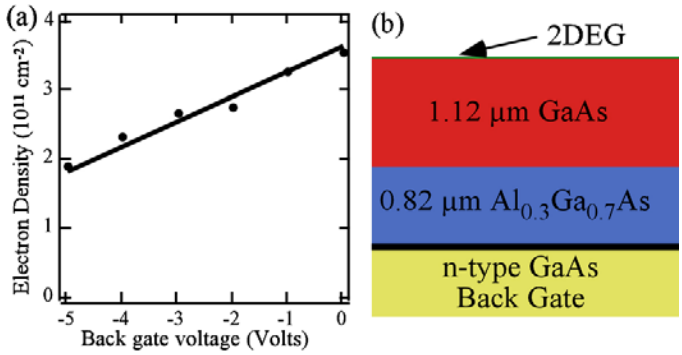

Figure 18. (a) Imaged density as a function of the back gate voltage. The circles were found using the FFT technique discussed in the text. The full line is the expected change in density from a capacitor model. This figure was reproduced with permission from [36]. Copyright 2002 American Institute of Physics. (b) Schematic diagram of the layers used in the capacitor model to calculate the expected change in density with back gate voltage.

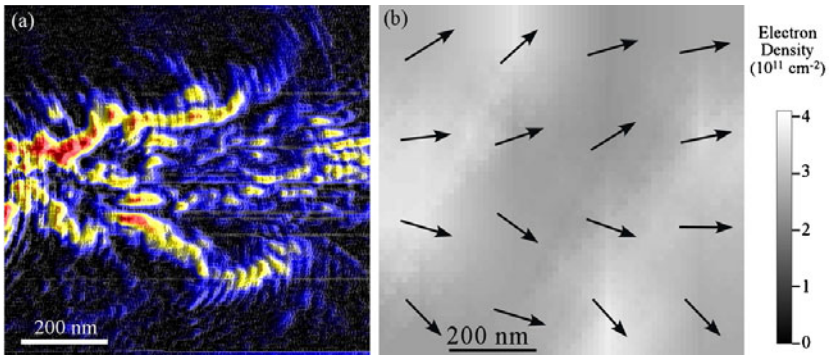

Figure 19. (a) Image of electron flow used to generate the map of electron density. (b) Map of the local electron density found using the FFT method described in the text. The arrows indicate the direction of electron flow at that location. This figure was reproduced with permission from [36]. Copyright 2002 American Institute of Physics.

more diffuse since the mobility, and hence the mean free path, is being reduced. Each branch of current is scattered and split into new branches more quickly since the mean free path is shorter. This leads to an image that no longer shows the narrow branches of current and instead becomes more uniform. For these experiments, we are interested in the spacing of the interference fringes as a function of back gate voltage.

6.3. Measuring local density

In order to measure the local electron density, the spacing of the interference fringes must be extracted while removing the background electron flow. Since the fringes are spaced by half the Fermi wavelength, there is a simple relation between their spacing, d, and the electron density, n. This relation is given by $n = \pi/(2d^2)$. A measurement of the density turns into a measurement of the spacing of the interference fringes. To isolate the interference fringes from the background flow, a spatial high pass filter is used. The high pass filtering was done by smoothing the data to remove the fringes and then subtracting this smoothed version from the

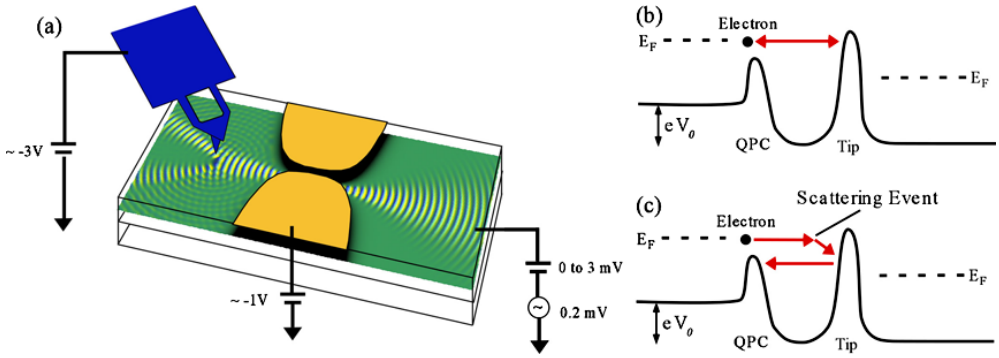

Figure 20. (a) Schematic diagram of the set-up used to image electron energy loss in the 2DEG. (b) Diagram showing that electrons injected with an excess energy can hit the tip and be backscattered through the QPC. (c) Same situation as in (b) except that the electron undergoes a scattering event in the round trip from the QPC to the tip and therefore cannot go back through the QPC. This will no longer contribute to the reduction in conductance. By measuring the decay of this signal as a function of distance from the QPC, the electron energy loss rate can be imaged.

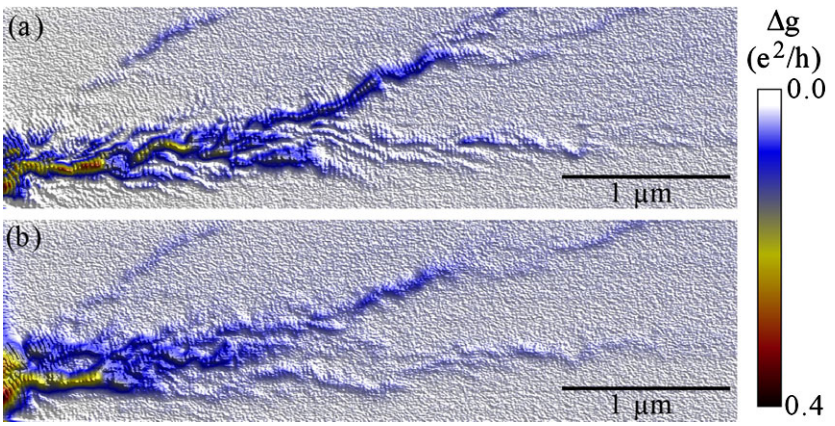

Figure 21. (a) Image of electron flow with no excess dc voltage across the QPC. (b) Image of electron flow with 2.4 mV dc voltage across the QPC. This voltage is added to the energy of the electrons and they lose it as they travel through the 2DEG. The signal grows fainter at long distances from the QPC in (b) as compared to that in (a), indicating that the electrons are losing their energy. This figure was reproduced with permission from [60]. Copyright 2002 IOP Publishing Limited.

original. The smoothing was done along the direction perpendicular to the fringes in order to reduce the fringe amplitude without changing the amplitude of the branches of electron flow. This filtering left only the high frequency components of the original image. This analysis was done for a small section of each scan to isolate the interference fringes. Figure 17 shows the high pass filtered images of electron flow from a small section of each image in figure 16. The back gate voltage for each image is as follows: (a) 0 V, (b) −1 V, (c) −3 V and (d) −5 V. As the back gate voltage becomes more negative, the spacing of the fringes clearly increases, indicating that the density is being reduced. These images no longer show any evidence of the background branches of electron flow.

To extract the spacing of the fringes from these images, a two-dimensional fast Fourier transform (FFT) was done on each image. This gives both the wavelength and direction of

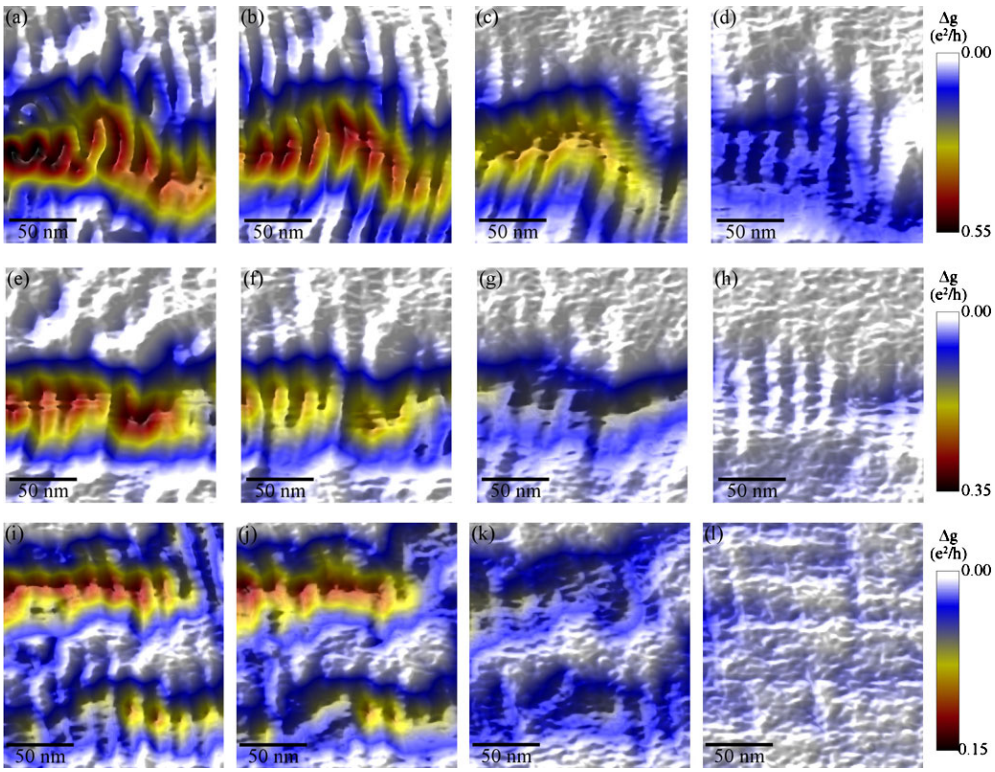

Figure 22. Images of electron flow at different distances from the QPC and dc bias voltages. (a)–(d) are at 0.6 μm from the QPC, (e)–(h) are at 1.0 μm and (i)–(l) are at 1.4 μm. The dc voltage across the QPC is as follows: (a), (e), (i) 0 mV, (b), (f), (j) 1 mV, (c), (g), (k) 2 mV and (d), (h), (l) 3 mV. As the distance or dc voltage increases the signal becomes fainter, indicating that the electrons are losing their excess energy.

the fringes. The fringes are oriented perpendicular to the direction of electron flow, so their direction gives information about the direction of electron flow. After performing the FFT, the location of the peak was found, giving the spacing of the interference fringes. This process was repeated for each of the scans to obtain the wavelength as a function of back gate voltage. The scans were taken in steps of -1 V on the back gate starting at 0 V. To convert the wavelength to density, we use the formula $n = \pi/2d^2$, where d is the fringe spacing. The density in each of the scans is plotted in figure 18(a) showing a linear decrease with back gate voltage starting slightly below 4.0×10^{11} cm^{-2}.

In order to compare the results with the expected change in density as a function of back gate voltage, we have used a simple parallel plate capacitor model. The conducting GaAs substrate, the back gate, is separated from the 2DEG by layers of GaAs and AlGaAs. Figure 18(b) shows the layers used in the capacitor model. This gives an expected change in density of 0.36×10^{11} cm^{-2} V^{-1} on the back gate. This is shown by the line in the plot of density versus back gate voltage in figure 18(a). The value of the density at 0 V is the one free parameter. This was chosen to produce the best match with the measured density using our imaging technique. This value is slightly lower than the value measured by Shubnikov–de Haas oscillations on another sample from the same wafer. There are several possible reasons for this slight difference, including the presence of the QPC gates, the charged cantilever and density variations within the sample.

6.4. Mapping electron density

To further investigate changes in density within a sample, images of the local electron density at several locations have been made to create a map of the local density. Figure 19(a) is an image of the electron flow showing the interference fringes with a back gate voltage of -1 V. The scan was divided into 16 parts and the density was found in each of these regions. Each of the regions used for creating the map was a circle with a radius of 100 nm. The regions were spaced by 200 nm. The density was found using the same procedure as in the previous section for the different back gate voltages. Figure 19(b) plots the measured density at each of the 16 locations. A linear interpolation was done between each of the points to produce the map of electron density. The arrows in the image represent the direction of electron flow at that location based on the direction of the fringes. From this map of electron density, we found an average density of 2.95×10^{11} cm^{-2}. This average density is in fairly good agreement with the previous imaging and Shubnikov–de Hass measurements. The measured density had a standard deviation of about 15%. This is fairly consistent with the simulations done by Shaw [38] of the expected variation in density due to the random placement and ionization of donor atoms.

In summary, a technique has been developed to image the local electron density in a 2DEG. The technique relies on measuring the interference fringes in images of electron flow to obtain the local Fermi wavelength and hence the density. Spatial variations in the density on a scale of about 100 nm can be imaged. The results for the change in density as a function of back gate voltage are in excellent agreement with a parallel plate capacitor model. We have also mapped the variation in the density due to the random ionization of donor atoms. The technique is useful for probing the complex density patterns that can be achieved with semiconductor growth and fabrication.

7. Imaging electron energy loss

In this section, a technique for measuring the electron–electron scattering rate in a 2DEG using an imaging technique is demonstrated. The ability to image electron energy loss is important for the design and understanding of new devices that rely on the coherence of the electron. There has been much experimental interest in studying the energy loss of electrons in 2DEGs through electron–electron scattering [62–65], electron–phonon scattering [66] and other mechanisms. However, in all of these experiments it has been very difficult to obtain spatial information about the scattering mechanisms. Most of the experiments have a fixed geometry, which does not allow for the study of the spatial dependence of the scattering without making multiple samples [62]. The ability to spatially image the energy loss may provide insight into the scattering mechanisms, like the ability to image electron flow providing evidence of branch formation in the 2DEG [17].

The design of new electronics devices that rely on the coherence of electrons has been an intense area of research. Determining the mechanisms that cause electrons to lose their coherence is important for a complete understanding of these devices. The technique of imaging electron flow is able to combine spatial information with transport measurements to provide more detail about these mechanisms. This allows the previous measurements of electron–electron scattering to be repeated with the addition of high resolution spatial information. The imaging technique also allows the measurement of the electron–electron scattering length in devices where the electron is confined to zero and one dimension. An understanding of the scattering mechanisms in each of these dimensions is necessary for the design and implementation of new quantum devices.

Previous theoretical work has shown that the electron–electron scattering time at zero temperature depends on the excess energy of the electron. As the energy increases the electron lifetime decreases approximately quadratically because there are more available states into which the electron can scatter [67]. This has been confirmed experimentally at distances shorter than the elastic mean free path by Yacoby *et al* [62]. For small excess energies, the lifetime also decreases with increasing temperature [68]. Fasol has extended the expression for the electron–electron scattering time to finite temperature and excess electron energy [69]. In the imaging experiment, the temperature is fixed but the excess energy of the electrons can be varied.

At the temperature and experimental parameters of our measurement, the electron–electron scattering length in the 2DEG is quite long, of the order of 20 μm. Since we are not able to image the flow over these large distances we have to shorten the electron–electron scattering length in our measurements. This is done by applying a dc voltage between the source and drain, which accelerates the electrons. They lose this extra energy through collisions with other electrons. Our results indicate that the dominant mechanism for energy loss at the temperatures and energies of the experiment is electron–electron scattering [60].

Section 7.1 describes the technique, which involves measuring the decay of the backscattered signal as a function of the applied source–drain voltage. Section 7.2 presents images of electron flow for different applied source–drain voltages. The images of electron flow show the signal decreasing for increasing source–drain voltage, indicating an increased scattering rate. Images are acquired as a function of distance and Fermi energy, showing increasing scattering with distance and decreasing Fermi energy. A comparison of all of the results with the theory for electron–electron scattering in a 2DEG is done in section 7.3. The results are in good agreement with the theory as a function of distance and energy.

7.1. Measurement technique

In the previous sections, a technique where the tip creates a depleted region of electrons that backscatters electron waves has been used. This produces a signal that is proportional to the electron flow at that location. In order to measure the energy relaxation, a new technique is needed that is sensitive to the energy of the electrons. Figure 20(a) illustrates the technique that is used to image the energy loss. A dc voltage V_0 is applied between the source and drain electrodes. This voltage accelerates the electrons as they go through the QPC. A fixed voltage is put on the tip with respect to the drain voltage, which scatters electrons hitting the depleted region under the tip. The voltage on the QPC gates is adjusted so that the highest energy electrons can just barely make it through the QPC, while ones that have less energy have to tunnel. A small ac signal is added to the dc voltage across the QPC to use for lock-in detection. This lock-in detection mechanism ensures that the measurement is only sensitive to electrons in a narrow energy band. An image of the conductance as a function of tip position is recorded.

In order to understand the images of electron flow, consider the following two cases: the electron goes from the QPC to the tip and back without losing any energy or it loses some energy on this round trip. In the first case, figure 20(b), the electron has not lost any energy and will be able to go back through the QPC. This backscattering will cause a reduction in the conductance when the tip is present. In the second case, figure 20(c), the electron loses energy during the round trip and can no longer go back through the QPC. Therefore, there will be no signal from this electron and no image of electron flow. By measuring the strength of the electron flow as a function of distance, the rate of electron energy loss is determined. The measurement of the electron flow is done by recording the differential conductance, $g = \partial I/\partial V_{ds}$, as a function

of tip position. We are interested in how much the flow changes when the tip is present so the relevant quantity is the change in differential conductance Δg. This is found by subtracting the signal when the tip is present from the signal without the tip. As the distance from the tip to the QPC increases, there is more time for the electron to lose energy and the signal should become weaker. The signal should also become weaker as the dc bias V_0 is increased because the electron has more available states to scatter into, which increases its scattering rate.

7.2. Images of electron flow

Figure 21 shows two images of electron flow from the same area. Figure 21(a) has no dc voltage V_0 applied across the QPC and figure 21(b) has $V_0 = 2.4$ mV applied across the QPC, which accelerates the electrons. In each image there is a small ac voltage of 0.2 mV used for lock-in detection. Near the QPC, the images have very similar contrast; the strength of the flow is similar in each image. However, at the furthest distances the 2.4 mV bias image is much weaker. This value of V_0 increases the rate at which electrons lose energy causing the image to be fainter at large distances. By measuring the decay of the signal as a function of distance, a determination of the electron scattering time is made. For a V_0 of 2.4 mV, the theoretical electron–electron scattering length is about 2.0 μm. This should give a decay of our signal by 63% at a distance of 1.0 μm because it is the round trip from the QPC to tip that is needed to produce the signal. It is also important to note that the interference fringes are present in both images showing that the measured flow is coherent. Because the fringes arise from an interference effect between different paths, a loss of coherence would destroy the interference effect. These interference fringes can give a measure of the electron energy because they are spaced by half the Fermi wavelength, as discussed in section 6 [36, 60].

To further investigate the distance dependence of the electron energy loss, three small regions of the electron flow have been examined. These are located at three different distances from the QPC. The closest one is at 0.6 μm, followed by 1.0 μm and the furthest is at 1.4 μm. Figure 22 shows the electron flow at these three locations for four different dc bias voltages V_0 at a temperature of 1.7 K. The colour scale is the change in differential conductance, Δg, for the given tip position. The distance from the QPC to the images is as follows: (a)–(d) 0.6 μm, (e)–(h) 1.0 μm and (i)–(l) 1.4 μm. Moving from left to right, V_0 goes from 0 up to 3 mV in steps of 1 mV. As the bias is increased the strength of the signal decreases for all three distances. However, it decreases much more quickly at the longest distance compared to the shortest one. At 1.4 μm and 3 mV, figure 22(l), we see almost no signal; it is primarily noise. This is in contrast to 0.6 μm and 3 mV, figure 22(d), where the signal is still quite strong. This shows that the electrons are losing their excess energy as they make the 2.8 μm round trip from the tip to the QPC in this image. However, in the shorter distance, the electron is less likely to undergo a scattering event and therefore the signal is not decaying as fast. To fully characterize the electron–electron scattering analysis of the signal as a function of excess applied energy is necessary.

A detailed study of the energy dependence of the signal was done by looking at the electron flow image as a function of the applied dc bias V_0. This was done at the same three locations as discussed earlier. To investigate the energy dependence, the average change in conductance was measured as a function of V_0. This average change $\overline{\Delta g}$ was found by averaging the measured signal over the entire scan area. This generates one data point for $\overline{\Delta g}$ for each value of V_0. Figure 23(a) plots this measured $\overline{\Delta g}$ versus bias voltage V_0. There are three sets of data for the three different distances. Each of the values in the plot has been normalized to the value without any dc bias. This means that each curve starts at 1 in the centre. The three curves have been offset from each other for clarity. In all three cases, the measured signal decreases with increasing energy. However, as the distance increases the signal decreases more quickly,

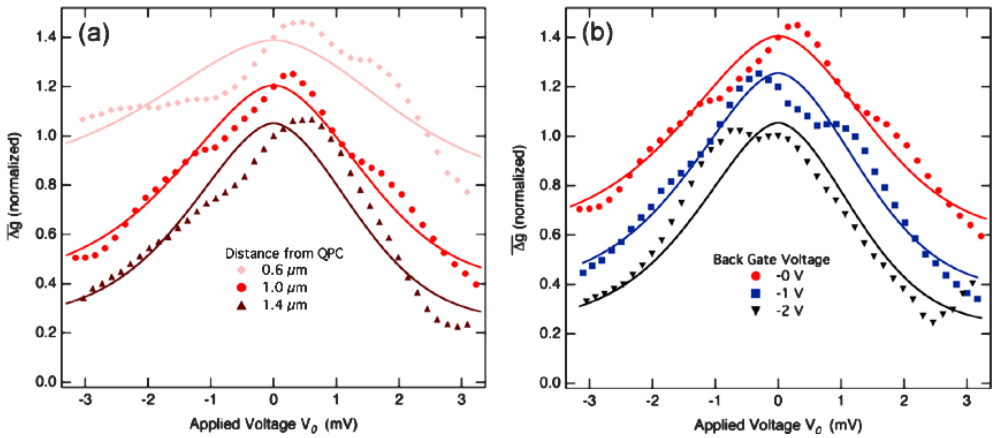

Figure 23. (a) Plot of the measured average change in conductance as a function of the excess dc voltage for the three distances shown in figure 22. (b) Plot of the measured average change in conductance as a function of dc voltage for three different back gate voltages. Each of these curves was taken at a distance of 1.0 μm from the QPC. The full curves in both figures are the expected decrease in signal due to electron–electron scattering. This figure was reproduced with permission from [60]. Copyright 2002 IOP Publishing Limited.

indicating that more scattering has occurred. This is in agreement with expectations because the electron has a longer time to scatter for the longer distances.

After studying the distance dependence of the electron–electron scattering, the effect of changing the Fermi energy of the electrons was examined. For a fixed excess energy, reducing the Fermi energy increases the scattering rate because the excess energy becomes a larger fraction of the total energy. This means more of the filled states may participate in the scattering, which increases the scattering rate. The measurements at the middle distance 1.0 μm have been repeated for a series of Fermi energies. In this case, the back gate voltage has been changed, which reduces the density of the 2DEG and lowers the Fermi energy. As the back gate voltage increases, the Fermi energy is reduced and the electron tends to scatter more quickly.

Figure 23(b) plots the measured average signal $\overline{\Delta g}$ as a function of dc bias voltage V_0 for three different back gate voltages. The points in the graph were obtained in the same manner as the ones in figure 23(a). Once again the curves have been offset and normalized to their value at $V_0 = 0$ mV. All three curves decrease with increasing dc bias voltage as expected from the increased scattering. The more important feature in this measurement is the back gate voltage dependence of the measured signal at a fixed V_0. The measured $\overline{\Delta g}$ is lower at a given V_0 for higher back gate voltages because V_0 is a larger fraction of the Fermi energy. This shows that the decreasing Fermi energy is increasing the scattering rate.

7.3. Theoretical scattering rate

In this section, we compare our results with a theoretical prediction for electron–electron scattering rate in a 2DEG. To understand the energy dependence for each of these three distances, we have looked at the expected electron–electron scattering rates in a 2DEG. This is the dominant scattering mechanism at these temperatures and energies in the 2DEG. Chaplik [67] and Giuliani and Quinn [68] have calculated the scattering time as a function of

the excess applied voltage V_0 at $T = 0$ K. They found the following equation for the scattering time, τ_{ee}:

$$\frac{1}{\tau_{ee}} = \frac{E_F}{4\pi\hbar}\left(\frac{eV_0}{E_F}\right)^2\left[\ln\left(\frac{E_F}{eV_0}\right) + \ln\left(\frac{2q_{TF}}{p_F}\right) + \frac{1}{2}\right].$$

In this equation, E_F is the Fermi energy, p_F is the momentum and q_{TF} is the Thomas–Fermi screening vector in two dimensions. This equation gives a good approximation of the electron–electron scattering rate as long as the excess energy is much larger than the temperature. This is true for our large bias voltages since $kT = 0.141$ meV. Since the measured signal $\overline{\Delta g}$ requires that the electron has not undergone a scattering event, the relevant quantity is the probability that an electron can travel a distance L without scattering. Because the chance of an electron scattering is random and they remain ballistic over the range of our measurement, the probability that an electron will not have scattered is given by the exponential decay

$$P \propto \exp\left(\frac{-L}{v\tau_{ee}}\right)$$

where v is the velocity after the electrons pass through the QPC and τ_{ee} is the scattering rate. This gives an approximately Gaussian distribution in the applied voltage V_0, since τ_{ee} goes as V_0^{-2}. The probability distribution is plotted in figure 23(a) for the three different distances from the QPC. There are no free parameters in the plotting of the probability distribution because L is given by the location of the image, the applied voltage V_0 is known and $E_F = 15$ meV is measured. There is qualitative agreement between the data and the expected distributions; the measured signal decays more quickly at longer distances. For the shortest distance, there is a larger discrepancy between the experiment and theory. This may be caused because the electrons have not been fully accelerated at such a short distance from the QPC. There is also an asymmetry in the bias direction, which may be caused by the shape of the QPC constriction.

The expected decrease in the signal as a function of V_0 for the three different back gate voltages has also been plotted. This is shown by the full curves in figure 23(b). As in the previous figure there are no free parameters in the fit of the expected versus measured distributions. The measured values for $L = 1.0$ μm, the applied voltage V_0 and Fermi energy E_F are used. Once again, there is good qualitative agreement between the experimental points and the theoretical curve, showing that electron–electron scattering is the dominant energy loss mechanism. The scattering rate increases as the Fermi energy decreases.

These measurements demonstrate the technique's ability to image electron energy loss in a 2DEG. This shows that, in our experiment, the dominant energy loss mechanism is electron–electron scattering. The results show good agreement between experiment and theory for the electron–electron scattering rate at a variety of distances and energies. This technique can be extended to measure electron energy loss mechanisms at higher excess energies where electron–phonon scattering becomes important. The technique can also be used in different geometries, like quantum wires and dots, to provide insight into the energy loss mechanisms in these confined geometries.

8. Conclusions

Scanning probe microscopy is a powerful tool for investigating the behaviour of electrons in a 2DEG. We have reviewed some recent experimental results on imaging electron flow through a 2DEG. We have shown images of the modal pattern of the electron wavefunctions near the QPC that are characterized by lobes determined by the width of the QPC. At further distances from the QPC, the images reveal the formation of narrow branches of current due to the small-angle scattering in the 2DEG. Images of electron flow have also been shown through a more

complicated device consisting of an electrostatic gate that acts as a prism for electrons passing underneath. The trajectories of electrons passing under the gate are bent by the applied voltage on the gate.

In the last half of the review, two techniques are discussed that have been developed for understanding electrons in the 2DEG. The first technique uses the interference fringes spaced by half the Fermi wavelength to measure the local electron density. The density in the 2DEG can be varied with a back gate voltage and the spacing of the fringes and electron density change as expected from a capacitor model. This technique is also able to profile spatial variations in the density on a length scale of about 100 nm. The second technique that is described is imaging electron energy loss in the 2DEG. A dc voltage is applied across the QPC to accelerate the electrons and, by imaging the distance travelled before losing their energy, the scattering rate in the 2DEG is measured. The measured length is in good agreement with theoretical predictions for the electron–electron scattering length.

Acknowledgments

The author is grateful to the many people who have worked on the experiments and theory described in this review. M A Topinka, A C Bleszynski, K E Aidala and R M Westervelt have worked on the imaging experiments. S E J Shaw, A Kalben and E J Heller have performed the quantum mechanical simulations of the electron flow. The semiconductor heterostructures were grown by K D Maranowski and A C Gossard. Financial support for this work was provided by the ONR grant N00014-95-1-0104 and the NSF Nanoscale Science and Engineering Center, grant PHY-0117795.

References

[1] Beenakker C W J and van Houten H 1991 Quantum transport in semiconductor nanostructures *Solid State Physics* vol 44, ed H Ehrenreich and D Turnbull (San Diego, CA: Academic) pp 1–228

[2] Sohn L L, Kouwenhoven L P and Schön G (ed) 1997 *Mesoscopic Electron Transport* (Boston, MA: Kluwer–Academic)

[3] Crommie M F, Lutz C P and Eigler D M 1993 Confinement of electrons to quantum corrals on a metal surface *Science* **262** 218

[4] Manoharan H C, Lutz C P and Eigler D M 2000 Quantum mirages formed by coherent projection of electronic structure *Nature* **403** 512

[5] Hudson E W, Pan S H, Gupta A K, Hg K-W and Davis J C 1999 Atomic-scale quasi-particle scattering resonances in $Bi_2Sr_2CaCu_2O_{8+\delta}$ *Science* **285** 88

[6] Pan S H, Hudson E W, Lang K M, Eisaki H, Uchida S and Davis J C 2000 Imaging the effects of individual zinc impurity atoms on superconductivity in $Bi_2Sr_2CaCu_2O_{8+\delta}$ *Nature* **403** 746

[7] Morgenstern M, Klijn J, Meyer C, Getzlaff M, Adelung R, Romer R A, Rossnagel K, Kipp L, Skibowski M and Weisendanger R 2002 Direct comparison between potential landscape and local density of states in a disordered two-dimensional electron system *Phys. Rev. Lett.* **89** 136806

[8] Morgenstern M, Klijn J, Meyer C and Weisendanger R 2003 Real-space observation of drift states in a two-dimensional electron system at high magnetic fields *Phys. Rev. Lett.* **90** 056804

[9] Lemay S G, Janssen J W, van den Hout M, Mooij M, Bronikowski M J, Willis P A, Smalley R, Kouwenhoven L P and Dekker C 2001 Two-dimensional imaging of electronic wavefunctions in carbon nanotubes *Nature* **412** 617

[10] Woodside M T and McEuen P L 2002 Scanned probe imaging of single-electron charge states in nanotube quantum dots *Science* **296** 1098

[11] Odom T W, Huang J-L and Lieber C M 2002 STM studies of single-walled carbon nanotubes *J. Phys.: Condens. Matter* **14** R145

[12] Eriksson M A, Beck R G, Topinka M, Katine J A, Westervelt R M, Campman K L and Gossard A C 1996 Cryogenic scanning probe characterization of semiconductor nanostructures *Appl. Phys. Lett.* **69** 671

[13] Topinka M A, LeRoy B J, Shaw S E J, Heller E J, Westervelt R M, Maranowski K D and Gossard A C 2000 Imaging coherent electron flow from a quantum point contact *Science* **289** 2323
[14] Crook R, Smith C G, Simmons M Y and Ritchie D A 2000 Imaging diffraction-limited electronic collimation from a non-equilibrium one-dimensional ballistic constriction *J. Phys.: Condens. Matter* **12** L167
[15] Crook R, Smith C G, Simmons M Y and Ritchie D A 2000 Imaging cyclotron orbits and scattering sites in a high-mobility two-dimensional electron gas *Phys. Rev.* B **62** 5174
[16] Crook R, Smith C G, Simmons M Y and Ritchie D A 2000 One-dimensional probability density observed using scanned gate microscopy *J. Phys.: Condens. Matter* **12** L735
[17] Topinka M A, LeRoy B J, Westervelt R M, Shaw S E J, Fleischmann R, Heller E J, Maranowski K D and Gossard A C 2001 Coherent branched flow in a two-dimensional electron gas *Nature* **410** 183
[18] Crook R, Smith C G, Simmons M Y and Ritchie D A 2001 Imaging random telegraph signal sites near a quasi 1D electron system *J. Phys.: Condens. Matter* **13** L249
[19] Woodside M T, Vale C, McEuen P L, Kadow C, Maranowski K D and Gossard A C 2001 Imaging interedge-state scattering centers in the quantum Hall regime *Phys. Rev.* B **64** 041310
[20] Crook R, Smith C G, Tribe W R, O'Shea S J, Simmons M Y and Ritchie D A 2002 Quantum-dot electron occupancy controlled by a charged scanning probe *Phys. Rev.* B **66** 121301
[21] Ihn T, Rychen J, Vancura T, Cilento T, Held R, Ensslin K, Wegscheider W and Bichler M 2002 Local spectroscopy of edge channels in the quantum Hall regime with local probe techniques *Physica* E **13** 671
[22] Ihn T, Rychen J, Cilento T, Held R, Ensslin K, Wegscheider W and Bichler M 2002 Scanning gate measurements on a quantum wire *Physica* E **12** 691
[23] Ihn T, Rychen J, Ensslin K, Wegscheider W and Bichler M 2002 Tunneling between edge channels in the quantum Hall regime manipulated with a scanning force microscope *Microelectron. Eng.* **63** 81
[24] Yoo M J, Fulton T A, Hess H F, Willett R L, Dunkleberger L N, Chichester R J, Pfeiffer L N and West K W 1997 Scanning single-electron transistor microscopy: imaging individual charges *Science* **276** 579
[25] Yacoby A, Hess H F, Fulton T A, Pfeiffer L N and West K W 1999 Electrical imaging of the quantum Hall state *Solid State Commun.* **111** 1
[26] McCormick K L, Woodside M T, Huang M, Wu M, McEuen P L, Duruoz C I and Harris J J 1999 Scanned potential microscopy of edge and bulk currents in the quantum Hall regime *Phys. Rev.* B **59** 4654
[27] Zhitenev N B, Fulton T A, Yacoby A, Hess H F, Pfeiffer L N and West K W 2000 Imaging of localized electronic states in the quantum Hall regime *Nature* **404** 473
[28] Ahlswede E, Weitz P, Weis J, von Klitzing K and Eberl K 2001 Hall potential profiles in the quantum Hall regime measured by a scanning force microscope *Physica* B **298** 562
[29] Ahlswede E, Weis J, von Klitzing K and Eberl K 2002 Hall potential distribution in the quantum Hall regime in the vicinity of a potential probe contact *Physica* E **12** 165
[30] Tessmer S H, Glicofridis P I, Ashoori R C, Levitov L S and Melloch M R 1998 Subsurface charge accumulation imaging of a quantum Hall liquid *Nature* **392** 51
[31] Finkelstein G, Glicofridis P I, Ashoori R C and Shayegan M 2000 Topographic mapping of the quantum Hall liquid using a few-electron bubble *Science* **289** 90
[32] Finkelstein G, Glicofridis P I, Tessmer S H, Ashoori R C and Melloch M R 2000 Imaging of low-compressibility strips in the quantum Hall liquid *Phys. Rev.* B **61** R16323
[33] Vogel M, Stein B, Pettersson H and Karrai K 2001 Low-temperature scanning probe microscopy of surface and subsurface charges *Appl. Phys. Lett.* **78** 2592
[34] Glicofridis P I, Finkelstein G, Ashoori R C and Shayegan M 2002 Determination of the resistance across incompressible strips through imaging of charge motion *Phys. Rev.* B **65** 121312
[35] Tessmer S H, Finkelstein G, Glicofridis P I and Ashoori R C 2002 Modeling subsurface charge accumulation images of a quantum Hall liquid *Phys. Rev.* B **66** 125308
[36] LeRoy B J, Topinka M A, Westervelt R M, Maranowski K D and Gossard A C 2002 Imaging electron density in a two-dimensional electron gas *Appl. Phys. Lett.* **80** 4431
[37] LeRoy B J 2003 Imaging coherent electron flow in semiconductor nanostructures *PhD Thesis* Harvard University
[38] Shaw S E J 2002 Propagation in smooth random potentials *PhD Thesis* Harvard University
[39] LeRoy B J, Bleszynski A C, Topinka M A, Westervelt R M, Shaw S E J, Heller E J, Maranowski K D and Gossard A C 2003 Imaging coherent electron wave flow in a two-dimensional electron gas *Physica* E **18** 163
[40] van Wees B J, van Houten H, Beenakker C W J, Williamson J G, Kouwenhoven L P, van der Marel D and Foxon C T 1988 Quantized conductance of point contacts in a two-dimensional electron gas *Phys. Rev. Lett.* **60** 848
[41] Wharam D A, Thornton T J, Newbury R, Pepper M, Ahmed H, Frost J E F, Hasko D G, Peacock D C, Ritchie D A and Jones G A C 1988 One-dimensional transport and the quantization of the ballistic resistance *J. Phys. C: Solid State Phys.* **21** L209–14

[42] Landauer R 1957 Spatial variation of currents and fields due to localized scatterers in metallic conduction *IBM J. Res. Dev.* **1** 223
[43] Landauer R 1970 Electrical resistance of disordered one-dimensional lattices *Phil. Mag.* **21** 863
[44] Büttiker M 1986 Four-terminal phase-coherent conductance *Phys. Rev. Lett.* **57** 1761
[45] He G P, Zhu S L and Wang Z D 2002 Conductance of a quantum point contact in the presence of a scanning probe microscope tip *Phys. Rev.* B **65** 205321
[46] Wolfson M A and Tomsovic S S 2001 On the stability of long-range sound propagation through a structured ocean *J. Acoust. Soc. Am.* **109** 2693
[47] Kaplan L 2002 Statistics of branched flow in a weak correlated random potential *Phys. Rev. Lett.* **89** 184103
[48] Vanicek J and Heller E J 2003 Uniform semiclassical wave function for coherent two-dimensional electron flow *Phys. Rev.* E **67** 016211
[49] Shaw S E J, Fleischmann R and Heller E J 2001 Quantum coherence beyond the thermal length *Preprint* cond-mat/0105354
[50] LeRoy B J, Bleszynski A C, Aidala K E, Westervelt R M, Kalben A, Heller E J, Maranowski K D and Gossard A C 2003 at press
[51] Topinka M A, LeRoy B J, Westervelt R M, Maranowski K D and Gossard A C 2002 Imaging coherent electron wave flow in a two-dimensional electron gas *Physica* E **12** 678
[52] Grill R and Dohler G H 1999 Effect of charged donor correlation and Wigner liquid formation on the transport properties of a two-dimensional electron gas in modulation delta-doped heterojunctions *Phys. Rev.* B **59** 10769
[53] Davies J H 1998 *The Physics of Low-Dimensional Semiconductors: an Introduction* (New York: Cambridge University Press)
[54] Spector J, Weiner J S, Störmer H L, Baldwin K W, Pfeiffer L N and West K W 1992 Ballistic electron optics *Surf. Sci.* **263** 240
[55] Spector J, Störmer H L, Baldwin K W, Pfeiffer L N and West K W 1990 Control of ballistic electrons in macroscopic two-dimensional electron systems *Appl. Phys. Lett.* **56** 967
[56] Spector J, Störmer H L, Baldwin K W, Pfeiffer L N and West K W 1990 Refractive switch for two-dimensional electrons *Appl. Phys. Lett.* **56** 2433
[57] Sivan U, Heiblum M, Umbach C P and Shtrikman H 1990 Electrostatic electron lens in the ballistic regime *Phys. Rev.* B **41** 7937
[58] Spector J, Störmer H L, Baldwin K W, Pfeiffer L N and West K W 1991 Noninteracting beams of ballistic two-dimensional electrons *Appl. Phys. Lett.* **58** 263
[59] Heremans J J, von Molnar S, Awschalom D D and Gossard A C 1999 Ballistic electron focusing by elliptic reflecting barriers *Appl. Phys. Lett.* **74** 1281
[60] LeRoy B J, Bleszynski A C, Topinka M A, Westervelt R M, Shaw S E J, Heller E J, Maranowski K D and Gossard A C 2003 Imaging coherent electron flow *Physics of Semiconductors 2002* ed A R Long and J H Davies (Bristol: Institute of Physics Publishing) pp 169–76
[61] Vancura T, Kicin S, Ihn T, Ensslin K, Bichler M and Wegscheider W 2003 Kelvin probe spectroscopy of a two-dimensional electron gas below 300 mK (*Preprint* cond-mat/0308069)
[62] Yacoby A, Sivan U, Umbach C P and Hong J M 1991 Interference and dephasing by electron–electron interaction on length scales shorter than the elastic mean free path *Phys. Rev. Lett.* **66** 1938
[63] Muller F, Lengeler B, Schäpers Th, Appenzeller J, Förster A, Klocke Th and Lüth H 1995 Electron–electron interaction in ballistic electron beams *Phys. Rev.* B **51** 5099
[64] Schäpers Th, Krüger M, Appenzeller J, Förster A, Lengeler B and Lüth H 1995 Effect of electron–electron interaction on hot ballistic electron beams *Appl. Phys. Lett.* **66** 3603
[65] Predel H, Buhmann H, Molenkamp L W, Gurzhi R N, Kalinenko A N, Kopeliovich A I and Yanovsky A V 2000 Effects of electron–electron scattering on electron-beam propagation in a two-dimensional electron gas *Phys. Rev.* B **62** 2057
[66] Sivan U, Heiblum M and Umbach C P 1989 Hot ballistic transport and phonon emission in a two-dimensional electron gas *Phys. Rev. Lett.* **63** 992
[67] Chaplik A V 1971 Energy spectrum and electron scattering in inversion layers *Zh. Eksp. Teor. Fiz.* **60** 1845
Chaplik A V 1971 *Sov. Phys.—JETP* **33** 997 (Engl. Transl.)
[68] Giuliani G F and Quinn J J 1982 Lifetime of a quasiparticle in a two-dimensional electron gas *Phys. Rev.* B **26** 4421
[69] Fasol G 1991 Electron dephasing due to Coulomb interaction *Appl. Phys. Lett.* **59** 2430